

PROGRESS REVIEW

Wafer-scale characterization for two-dimensional material layers

To cite this article: A. Moussa *et al* 2024 *Jpn. J. Appl. Phys.* **63** 030802

View the [article online](#) for updates and enhancements.

You may also like

- [Senior high school student's visual-spatial intelligence according to van hiele geometric thinking theory](#)
Y Y Wijaya, Sunardi, Slamin et al.
- [Interface Engineering of Next Generation Lithium Metal Anodes](#)
Malachi Noked, Alexander C Kozen, Marshall A Schroeder et al.
- [\(Invited\) Electron Channeling Contrast Imaging for Rapid Characterization of Compound Semiconductors](#)
Julia Deitz, Timothy Ruggles, Stephen Lee et al.



Wafer-scale characterization for two-dimensional material layers

A. Moussa^{1*}, J. Bogdanowicz¹, B. Groven¹, P. Morin¹, M. Beggiato¹, M. Saib¹, G. Santoro², Y. Abramovitz³, K. Houchens³, S. Ben Nissim³, N. Meir⁴, J. Hung⁴, A. Urbanowicz⁴, R. Koret⁴, I. Turovets⁴, B. Lee⁵, W.T. Lee⁵, G. F. Lorusso¹, and A.-L. Charley¹

¹Imec, 3001 Leuven, Belgium

²Applied Materials, 3001 Leuven, Belgium

³Applied Materials, Rehovot, Israel

⁴Nova Measuring Instruments Inc., Rehovot 7632805, Israel

⁵Nova Measuring Instruments Inc., Fremont, CA 93117, United States of America

*E-mail: alain.moussa@imec.be

Received December 6, 2023; revised January 22, 2024; accepted February 5, 2024; published online March 11, 2024

Logic devices based on two-dimensional (2D) channel materials require highly crystalline monolayers. Despite various laboratory-scale metrology techniques being intensively used to characterize 2D materials on small coupons, the development of in-line and routine characterization of 2D material monolayers grown on 300 mm wafers remains in its early stages. In this work, we evaluate and combine different in-line metrologies to characterize the thickness and morphology of tungsten disulfide (WS₂) monolayers at the 300 mm wafer level. By combining complementary metrology techniques, we reveal the morphology of WS₂, the WS₂ layer thickness and within-wafer uniformity for different WS₂ deposition conditions across 300 mm wafers. © 2024 The Japan Society of Applied Physics

1. Introduction

The next extension of Moore's law will occur through a multitude of approaches. Beyond the traditional scaling and new three-dimensional device architectures, potential logic device scaling roadmaps also foresee a transition from Si to atomically thin and disruptive channel materials, such as two-dimensional (2D) materials.¹⁾ In particular, the semiconducting transition metal dichalcogenides (TMDs), such as molybdenum disulfide (MoS) and tungsten disulfide (WS₂), combine relevant material properties to overcome short-channel effects when device gate lengths are squeezed below 10 nm.²⁻⁵⁾ However, fabricating such high-performance devices requires 2D channel materials of high crystalline quality with monolayer thickness and crystal defect control.⁶⁻¹⁰⁾ For example, the electronic bandgap and transport behaviour vary strongly with the number of TMD monolayers and crystalline defects.^{11,12)} To date, the development of in-line characterisation for TMD monolayers integrated on 300 mm wafers remains in the early stages, and it is essential to be able to probe the morphology, crystallinity and thickness of TMD monolayers routinely, in an automated manner and with high statistical confidence. In-line metrology provides vital understanding on how to design and engineer key process modules for the integration of 2D materials, such as TMD channel deposition and transfer, and gate-stack deposition and contact fabrication.

Therefore, here we evaluate and combine different in-line metrologies to characterise at wafer level the thickness and morphology of WS₂ monolayers deposited on 300 mm wafers.¹³⁾ We used a set of five wafers with different WS₂ surface coverages ranging from a non-closed monolayer to several monolayers. Subsequently, these wafers were characterised using five in-line techniques. First, atomic force microscopy (AFM) provides the WS₂ topography, surface roughness and layer step height. Second, scanning electron microscopy (SEM) reveals the surface coverage of the individual WS₂ monolayers via their contrast in the SEM images. Two optical metrologies, scatterometry and Raman spectroscopy, provide information about the average WS₂

thickness and morphology. Finally, X-ray photoelectron spectroscopy (XPS) brings information about the chemical bonding structure and state of WS₂. Combining the results from these five complementary in-line characterisation techniques quantifies the WS₂ morphology, layer thickness and within-wafer uniformity across 300 mm wafers for different WS₂ deposition conditions.

2. Experimental

Due to the very thin structure of WS₂, metrology remains difficult. Indeed, a monolayer of WS₂ has a thickness of less than 1 nm. Given the atomic resolution of AFM in the Z direction, this is our first candidate for measuring the topography and thickness of the layer. However, as we want to characterize the layer across the 300 mm wafer, the AFM throughput remains too low to perform this in a decent time. SEM has been used to manage throughput and characterize the layer coverage and uniformity on the wafer. The other techniques evaluated in this work are optical metrology, scatterometry and Raman analysis. They provide information about the thickness and morphology of the layer.

2.1. WS₂ deposition

WS₂ is deposited by metal-organic CVD (MOCVD) on 300 mm Si substrates covered with a thermally grown SiO₂ layer. The WS₂ MOCVD process utilises tungsten hexacarbonyl (W(CO)₆) and dihydrogen sulfide (H₂S) as the transition metal and sulfur precursor, respectively, in an industry-standard yet customised 300 mm epitaxial and horizontal single-wafer CVD reactor. The amount of deposited WS₂ is varied by increasing the MOCVD deposition time for wafers labelled as A, B and C.

2.2. Atomic force microscopy

AFM is a type of scanning probe microscopy. The measurement is performed directly by recording the deflection of a laser spot reflected on a probe scanning on top of the sample. This setup has atomic resolution in the Z direction. In this work, the measurements were performed with a Park Systems NX3DM tool in 'true non-contact' mode,¹⁴⁾ which causes less damage to the sample and increases the probe lifetime. As the throughput of AFM is low, only six measurements of areas of

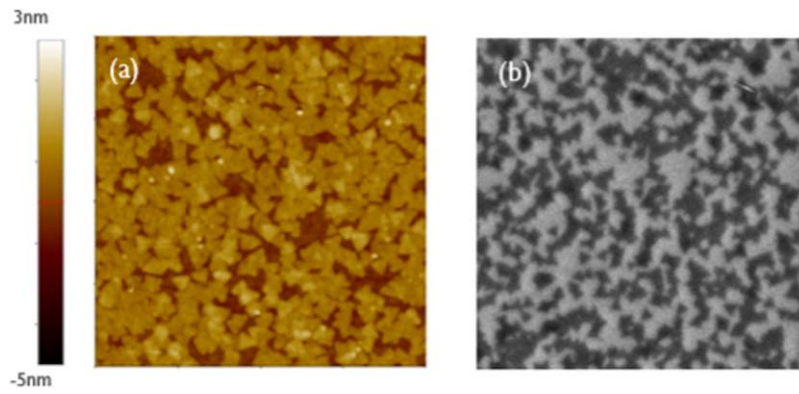


Fig. 1. Image of a $1 \mu\text{m} \times 1 \mu\text{m}$ area (a) from an AFM image with the z-scale on the right and (b) from a SEM image.

$1 \mu\text{m} \times 1 \mu\text{m}$ were made per wafer (Fig. 1a), from the centre to the edge of the wafer. Each image was flattened with a first-order regression. Histogram analysis of the images provides the topography and thickness of the layer.

2.3. SEM

SEM analysis of the layer across the wafer was realised with a tool from Applied Materials. Acquisition conditions were tuned to optimise the contrast between the substrate, monolayer and multiple layers of WS_2 . Thanks to the throughput of the tool, 89 images of a $1 \mu\text{m} \times 1 \mu\text{m}$ area were acquired across each wafer (Fig. 1b). The analysis of the images provides the coverage area of the substrate, monolayer and multiple layers of WS_2 in each image.

2.4. Scatterometry

Scatterometry is an optical model-based technique suitable for the characterisation of layer thickness.^{15–17} The same wafer map as for SEM was used for the analysis across the wafer with a shift to avoid possible damage from other techniques. The Nova MMSR scatterometry tool used in this work exploits a wide range of wavelengths at multiple azimuths and angles of incidence. Reconstruction of the spectrum by modelling provides the thickness of the WS_2 layer averaged over the spot area. Figure 2(a) shows the

spectrum from the reference sample and sample with a monolayer (A), this reveals the sensitivity of the scatterometry.

2.5. Raman analysis

Raman spectra were acquired on the Nova ELIPSON™ tool. This analysis was done on each wafer with a 45-point wafer map. As described in the literature,¹⁸ the position and intensity of the E_{2g} and A_{1g} peaks in the Raman spectrum provide information about the layer thickness and morphology across the wafer. As in most optical metrology methods, the signal is averaged over the spot area. Figure 2(b) shows Raman spectra for samples with one and two monolayers.

2.6. X-ray photoelectron spectroscopy

XPS spectra were acquired on the Nova Veraflex™ tool. XPS is a surface chemical analysis method. The sample is irradiated with an X-ray beam and electrons are extracted from the surface. The energy and number of electrons extracted are characteristic of the binding of the element and its quantity in the layer, respectively. Analysis of the spectrum therefore provides the quantity of an element and its bonding state¹⁹. Figure 2(c) shows XPS spectra for different samples.

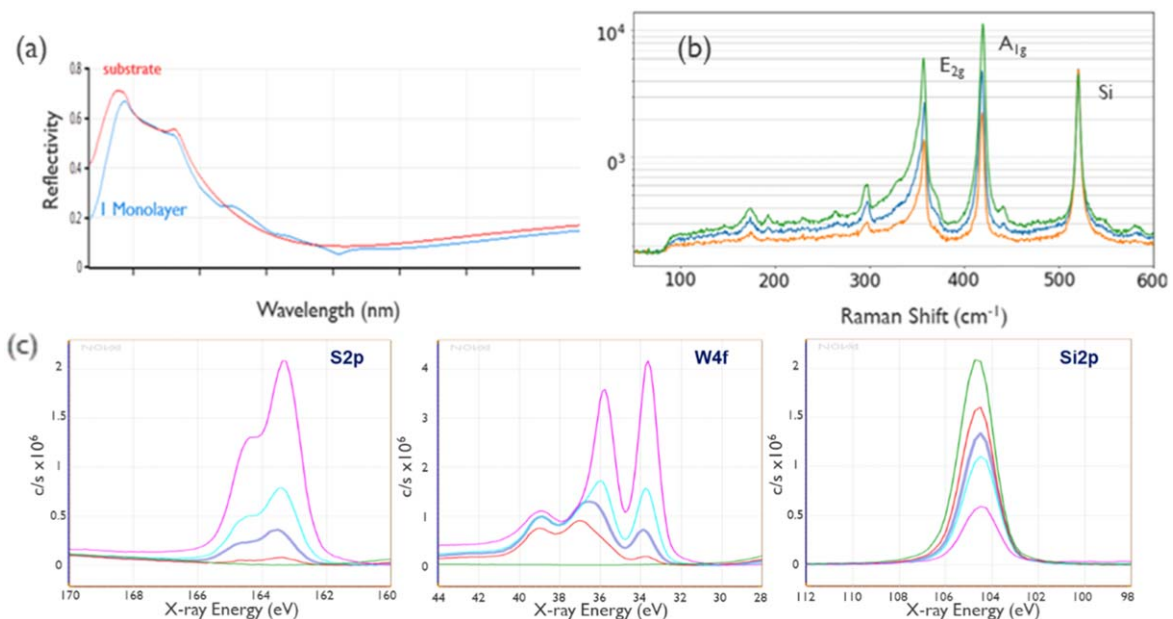


Fig. 2. (a) Scatterometry spectrum for substrate (red) and a monolayer of WS_2 on the substrate (blue). (b) Raman and (c) XPS spectra for WS_2 layers with different thicknesses.

3. Results and discussions

In this section we show and discuss the results of each measurement method on a set of 300 mm wafers corresponding to four unique WS₂ MOCVD deposition conditions. One sample (A) consists of a continuous and primarily monolayer-thin WS₂ layer deposited using process-of-record MOCVD deposition conditions. For samples B and C the WS₂ layer thickness and surface coverage have been intentionally altered via the MOCVD deposition time to produce sub-monolayer WS₂ and several layers of deposited WS₂, respectively. The fourth and last wafer (D) consists of large and isolated crystals of WS₂ on a bare SiO₂ initial surface. Combination and correlation of the results for the different metrologies make it possible to describe the layer of 2D material for each sample.

3.1. AFM and SEM

AFM provides the true height distribution of the layer^{20–23} while SEM provides grayscale contrast of the layer. The AFM and SEM images of the same isolated island (D) allow us to attribute the different contrasts in the SEM image to the layer thickness in the AFM image (Fig. 3).

Therefore, the peaks in the histogram analysis of AFM and SEM images (Fig. 1) can be attributed to the substrate (i.e. the initial SiO₂ surface), the first WS₂ monolayer and the number of WS₂ monolayers on top of the basal plane of the first WS₂ monolayer. Figure 4 shows the histogram analysis of each sample for AFM and SEM images. The coloured boxes show the range of height and grayscale assigned to the different WS₂ layer thicknesses, from the starting surface or substrate (red), the first monolayer (green), and the monolayers on top of the basal plane of the first monolayer (blue).

Histogram analysis from SEM images allows us to optimise the threshold to discriminate the layers thickness from zero or one monolayer and more than one monolayer. A homemade segmentation algorithm²⁴ calculates per image the coverage area of each grey scale range. Figure 5 shows, for each kind of sample, an SEM image and its segmentation.

The results of this image analysis allow us to create 300 mm wafer maps of the surface coverage for each height range and as a function of the wafer radius (Fig. 6). Figure 6 shows the layer uniformity for sample A and a radial trend for samples B and C. This is because sample B has mostly a monolayer with less coverage in the centre than near the edge and sample C has the same trend but starting, mostly, from a single layer in the centre to a multilayer near the edge.

3.2. Scatterometry

As mentioned in Sect. 2.4, Scatterometry provides the average thickness of the WS₂ layer in the spot area.

Figure 7 shows the scatterometry results, as wafer map, for samples A, B and C. For each sample a radial trend is visible, but if sample A has a thicker layer in the centre, samples B and C show the opposite. Furthermore, sample A is more homogeneous than samples B and C.

These results can be compared with the results of SEM image analysis. In the SEM images the amount of WS₂ can be evaluated by the sum of the monolayer coverage and twice the multilayer coverage. Figure 8 shows this correlation: the correlation coefficient between this calculation and the scatterometry result is equal to 0.9981, which confirms that the 2D analysis of the SEM image agrees with the average thickness measured via scatterometry.

3.3. Raman analysis

As mentioned in Sect. 2.5, the intensity and position of the E_{2g}, A_{1g} and Si peaks in the Raman spectrum provide information about the WS₂ crystal lattice and layer thickness. Figure 9 shows a boxplot of the intensity and position of these peaks for all measurements per sample. The intensity of the peaks correlates with the thickness of the WS₂ layer. Indeed, the intensity of the E_{2g} and A_{1g} peaks increases with thickness when the intensity of the Si peak decreases. This decrease can be explained by the shielding of the substrate by the WS₂ layer when its thickness increases. Also, whatever the thickness of the WS₂ layer, the position of the Si peak is not affected but the positions of the A_{1g} and E_{2g} peaks are. In fact, the position of the A_{1g} peak increases with the number of layers. This is explained by the fact that samples A and B mainly have a monolayer of WS₂ and sample C mainly a bilayer. On the contrary, the position of the E_{2g} peak decreases with the type of process and the number of layers. As described in literature,^{25,26} the difference in the E_{2g} peak position for samples with a monolayer can be explain by the difference in strain in the layer due to the deposition process.

To demonstrate the correlation between the thickness of the layer and the intensity of the A_{1g} and E_{2g} peaks, Fig. 10 shows a correlation plot between the thickness of the WS₂ layer obtained by scatterometry and the intensity of the peak collected at the same site for the three samples. A correlation coefficient higher than 0.99 confirms that the intensity of the A_{1g} and E_{2g} peaks corresponds to the amount of WS₂.

3.4. XPS analysis

As for previous metrologies, XPS is sensitive to the amount of WS₂ and so to the layer thickness.^{27,28} This can be shown by the correlation between the integration of the peaks for W 4f and the thickness of the WS₂ layer obtained by scatterometry (Fig. 11b). Additionally, because XPS is a surface analysis, the Si–O signal will decrease with increase in the

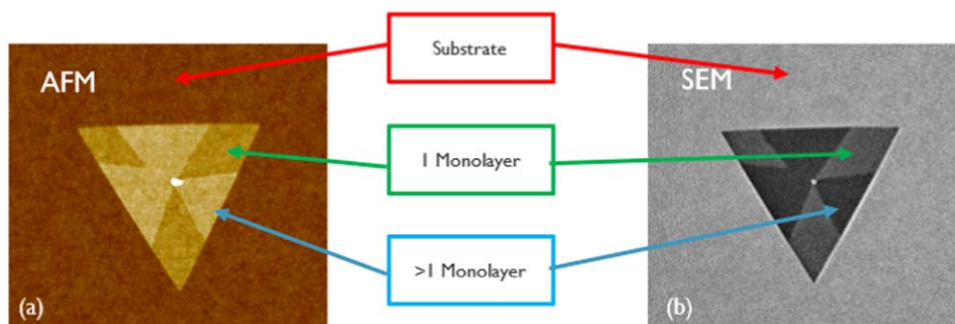


Fig. 3. 4 $\mu\text{m} \times 4 \mu\text{m}$ image of an isolated island of WS₂ (a) from AFM and (b) from SEM.

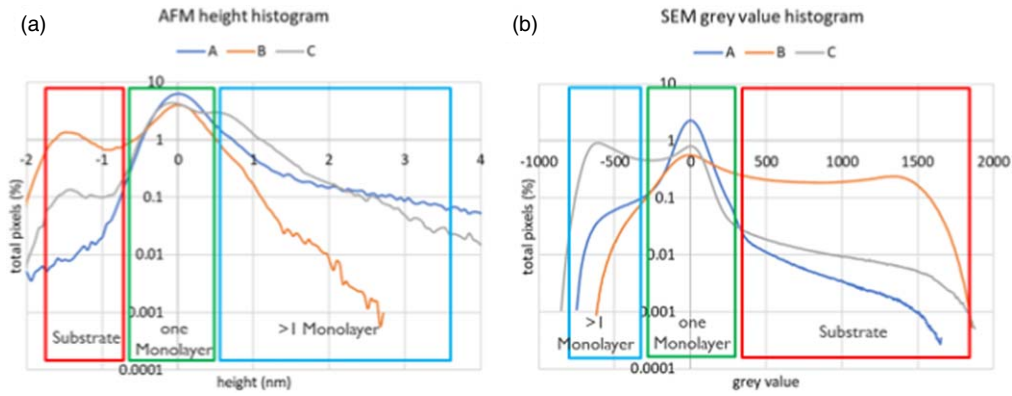


Fig. 4. Histogram overlay for an image of samples A, B and C from (a) AFM and (b) SEM. Note: the histograms are aligned to the peak assigned to the monolayer.

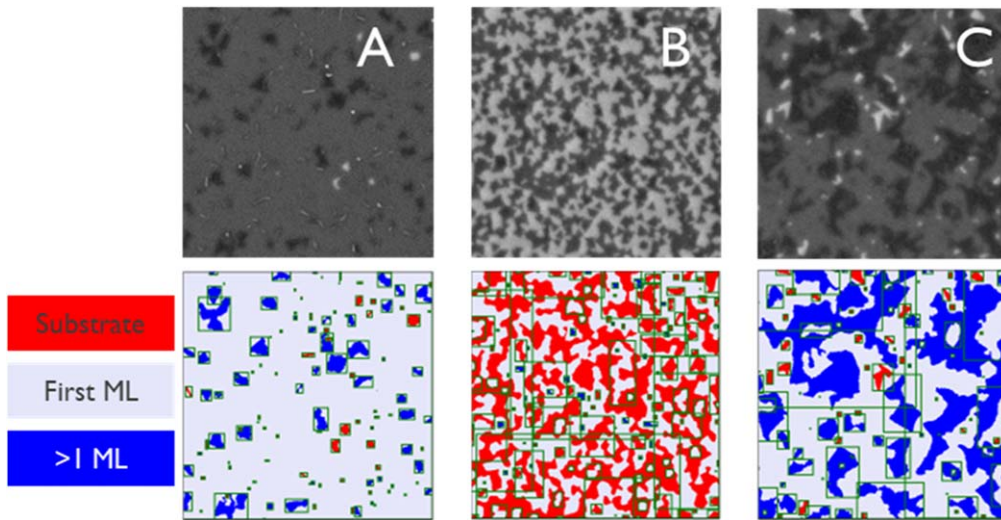


Fig. 5. $1 \mu\text{m} \times 1 \mu\text{m}$ SEM images (top) and their segmentation result (bottom) (ML, monolayer).

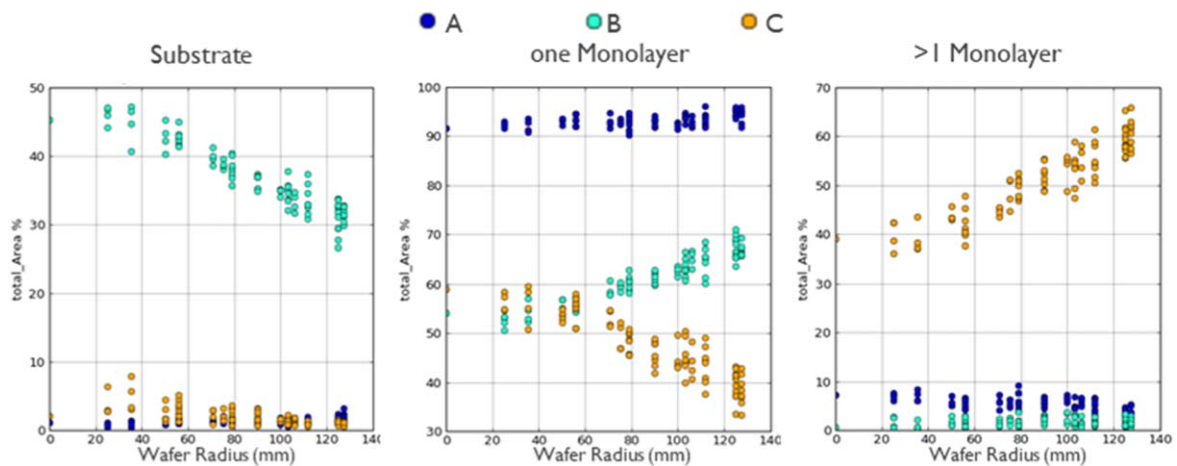


Fig. 6. Percentage coverage per step height for samples A, B and C versus the wafer radius: left, substrate; centre, one monolayer; right, more than one monolayer.

thickness of the layer above. The thickness of the WS_2 layer can therefore be evaluated from the extinction of the Si-O signal (Fig. 11a). However, the most interesting analysis available in the XPS spectrum is the identification of element bonds. Figure 2(c) (centre) shows the peaks for the 4f electron of W. This spectrum shows a double band for the W-S and W-O bonds. Deconvolution of the peaks allows us to quantify the ratio between W-O and W-S. This analysis shows that the

W in the thinnest layer is 82% oxidised for sample A and 95% for sample B, but for sample C the ratio is around 50% (Fig. 11c). These results show that XPS is sensitive to elemental state and can help us understand the impact of process steps on the WS_2 layer. Unfortunately, in this case the oxidation of the outer layer of WS_2 is certainly due to the aging of the sample; in fact the XPS spectra were acquired well after the measurements with the previous methods.

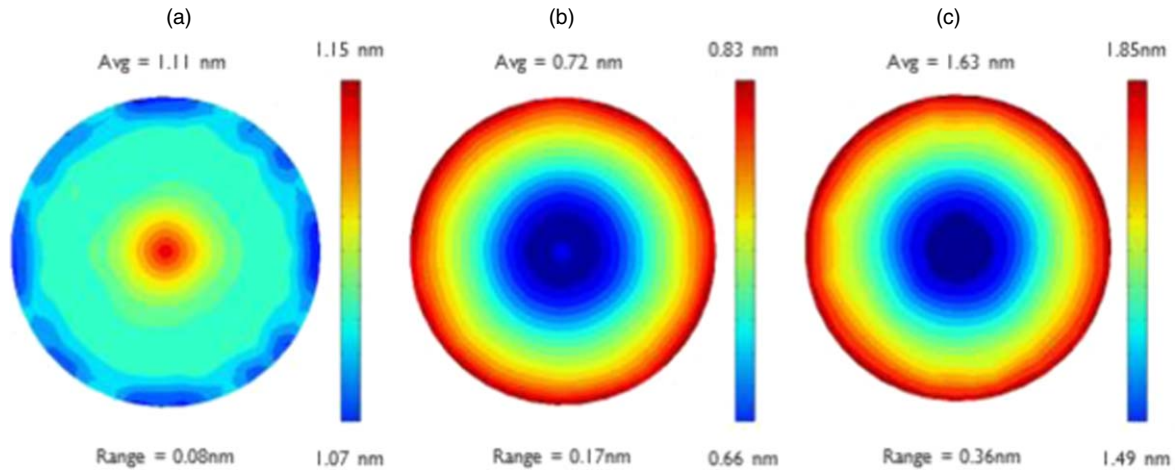


Fig. 7. Scatterometry results: average thickness of the layer of WS₂ for (left to right) samples A, B and C.

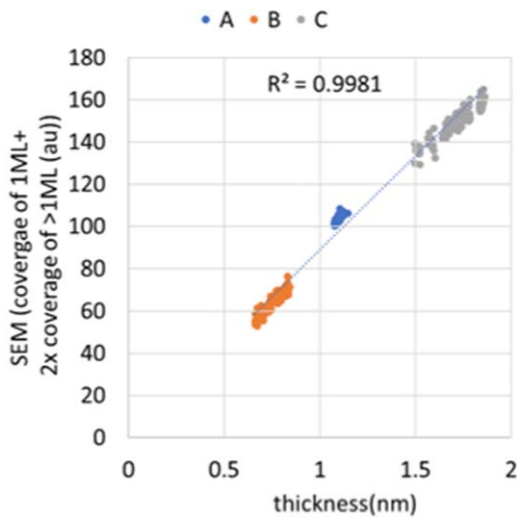


Fig. 8. Correlation between scatterometry results and SEM image analysis for samples A, B and C. The correlation coefficient was calculated for all the data (ML, monolayer).

4. Summary and conclusions

This work evaluated and demonstrated that complementary and in-line measurement methods can probe and characterize the thickness and morphology of a single WS₂ monolayer at the 300 mm wafer level. First, in-line AFM quantifies the layer thickness, topography and surface roughness for WS₂ for surface coverages ranging from sub-monolayer to multi-layer. Moreover, by correlation with SEM, this analysis can be extended to full 300 mm wafer maps within a relevantly short amount of acquisition and analysis time. In-line SEM emerges as a routine characterisation to extract with high statistical confidence figures of merit that could provide insight into elementary processes and mechanisms during the WS₂ deposition process. Second, scatterometry is a fast method for measuring full 300 mm wafer maps of the average WS₂ layer thickness based on an optical model. There is an excellent correlation between the average WS₂ thickness as determined by scatterometry and the calculated thickness

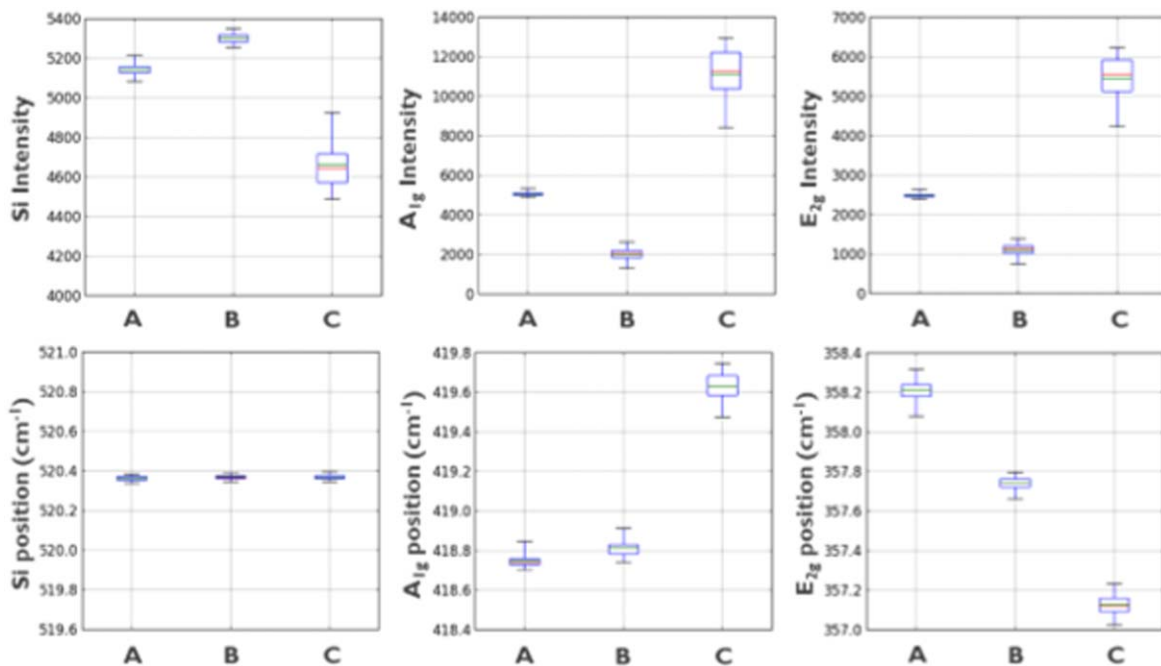


Fig. 9. Box plots of intensity (top) and position (bottom) of the Si, A_{1g} and E_{2g} peaks with 45 points per sample.

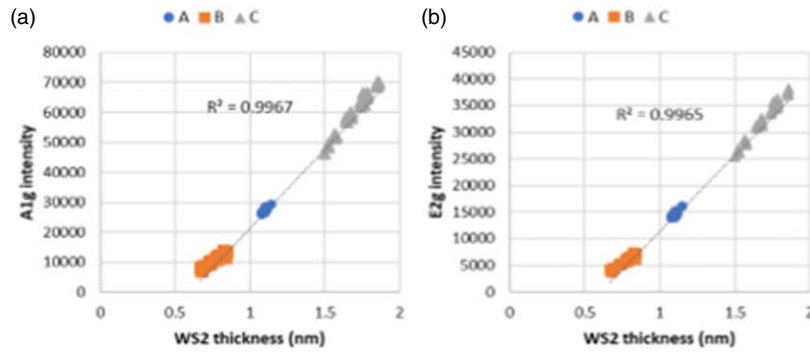


Fig. 10. Correlation between WS₂ layer thickness obtained via scatterometry and the intensity of the (a) A_{1g} and (b) E_{2g} peaks from the Raman spectra.

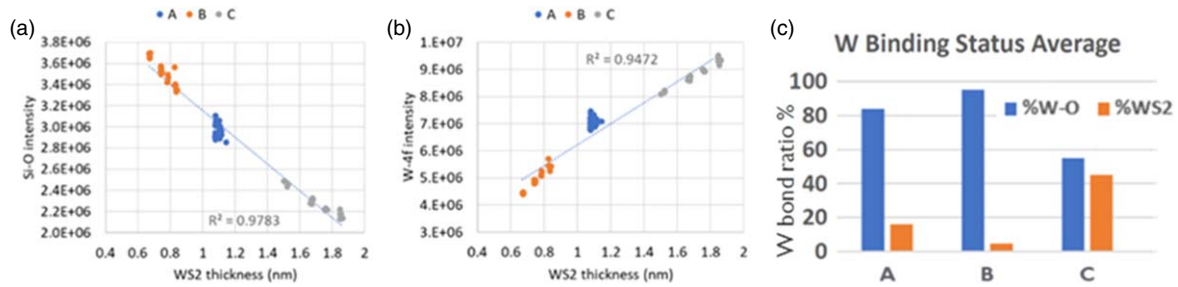


Fig. 11. Correlation between WS₂ layer thickness obtained via scatterometry and the intensity of the (a) Si–O and (b) W 4f peaks from the XPS spectrum. (c) Ratio of W bonds to S or O per sample.

based on the WS₂ surface coverage from SEM. Third, Raman optical metrology analysis further correlates to the average thickness by means of the A_{1g} and E_{2g} optical vibrational modes. The peak position provides information on the WS₂ morphology: a blueshift of the A_{1g} peak hints at the deposition of several WS₂ monolayers, whereas the redshift of the E_{2g} peak suggests the effect of the process on the strain in the layer. Finally, XPS is sensitive to the layer thickness and depicts the chemical bonding structure and oxidation state of W in the WS₂ monolayer as well as the compositional ratio. Further fundamental exploration of in-line characterisation techniques for 2D materials promises to significantly accelerate the number of learning cycles in terms of throughput and statistical analysis, thus guiding the rational design of key process modules for the integration of 2D materials in logic devices.

ORCID iDs

A. Moussa <https://orcid.org/0000-0002-6377-4199>

- 1) L. Van den Hove, “The endless progression of Moore’s law,” Proc. SPIE PC12053, Metrology, Inspection, and Process Control XXXVI; PC1205302022, [10.1117/12.2606055](https://doi.org/10.1117/12.2606055).
- 2) S. Manzeli et al., “2D Transition metal dichalcogenides,” *Nat. Rev. Mater.* **2**, 1 (2017).
- 3) C. Huyghebaert et al., “2D Materials: roadmap to CMOS integration,” IEEE Int. Electron Devices Meeting (IEDM), 2018, p. 22.1.1, [10.1109/IEDM.2018.8614679](https://doi.org/10.1109/IEDM.2018.8614679).
- 4) T. Agarwal et al., “Benchmarking of monolithic 3D integrated MX₂ FETs with Si FinFETs,” IEEE International Electron Devices Meeting (IEDM) 2017, p. 5.7.1, [10.1109/IEDM.2017.8268336](https://doi.org/10.1109/IEDM.2017.8268336).
- 5) Q. Smets et al., “Ultra-scaled MOCVD MoS₂ MOSFETs with 42nm contact pitch and 250 μA/μm drain current,” IEEE Int. Electron Devices Meeting (IEDM) (San Francisco, CA, USA), 2019, p. 23.2.1, [10.1109/IEDM19573.2019.8993650](https://doi.org/10.1109/IEDM19573.2019.8993650).

- 6) K. P. O’Brien, “Are 2D transition metal dichalcogenides transistors the future silicon replacement or hype?,” Proc. SPIE 12498, Advances in Patterning Materials and Processes XL, 1249802, 2023, [10.1117/12.2669891](https://doi.org/10.1117/12.2669891).
- 7) K. P. O’Brien et al., “Process integration and future outlook of 2D transistors,” *Nat. Commun.* **14**, 6400 (2023).
- 8) D. Akinwande et al., “Graphene and two-dimensional materials for silicon technology,” *Nature* **573**, 507 (2019).
- 9) Y. C. Lin et al., “Recent advances in 2D material theory, synthesis, properties, and applications,” *ACS Nano* **17**, 9694 (2023).
- 10) I. Asselberghs et al., “Scaled transistors with 2D materials from the 300 mm Fab,” IEEE Silicon Nanoelectronics Workshop (SNW), 2020, p. 67, [10.1109/SNW50361.2020.9131651](https://doi.org/10.1109/SNW50361.2020.9131651).
- 11) A. Splendiani et al., “Emerging photoluminescence in monolayer MoS₂,” *Nano Lett.* **10**, 1271 (2010).
- 12) T. H. Ly et al., “Misorientation-angle-dependent electrical transport across molybdenum disulfide grain boundaries,” *Nat. Commun.* **7**, 10426 (2016).
- 13) A. Moussa et al., “300 mm in-line metrologies for the characterization of ultra-thin layer of 2D materials,” Proc. SPIE 12496, Metrology, Inspection, and Process Control XXXVII, 124961X, 2023, [10.1117/12.2657968](https://doi.org/10.1117/12.2657968).
- 14) J. Paul Pineda et al., “High resolution imaging of particles dispersed in polymeric matrix by true non-contact™ mode atomic force microscopy,” *NanoSci. Mag.* **18**, 13 (2020).
- 15) H-L. Liu et al., “Optical properties of monolayer transition metal dichalcogenides probed by spectroscopic ellipsometry,” *Appl. Phys. Lett.* **105**, 201905 (2014).
- 16) M. Magnozzi et al., “Local optical properties in CVD-grown monolayer WS₂ flakes,” *Phys. Chem. C* **125**, 16059 (2021).
- 17) G. A. Ermolaev et al., “Spectroscopic ellipsometry of large area monolayer WS₂ and WSe₂ films,” *AIP Conf. Proc.* **2359**, 020005 (2021).
- 18) L. Liang et al., “First-principles raman spectra of MoS₂, WS₂ and their heterostructures,” *Nanoscale* **6**, 5394 (2014).
- 19) R. Scarfello et al., “An insight into chemistry and structure of colloidal 2D-WS₂ nanoflakes: combined XPS and XRD study,” *Nanomaterials* **11**, 1969 (2021).
- 20) K. Godin, C. Cupo, and E. H. Yang, “Reduction in Step Height Variation and Correcting Contrast Inversion in Dynamic AFM of WS₂ Monolayers,” *Sci. Rep.* **7**, 17798 (2017).
- 21) K. Kang, K. Godin, and E. H. Yang, “The growth scale and kinetics of WS₂ monolayers under varying H₂ concentration,” *Sci. Rep.* **5**, 13205 (2015).
- 22) P. K. Nayak et al., “Layer-dependent optical conductivity in atomic thin WS₂ by reflection contrast spectroscopy,” *ACS Appl. Mater. Interfaces* **6**, 16020 (2014).

- 23) C. Cong et al., "Synthesis and optical properties of large-area single-crystalline 2D semiconductor WS₂ monolayer from chemical vapor deposition," *Adv. Opt. Mater.* **2**, 131 (2014).
- 24) S. Saib et al., "Advanced characterization of 2D materials using SEM image processing and machine learning," SPIE-ALPProc. SPIE 12955, Metrology, Inspection, and Process Control XXXVIII, 2024.
- 25) F. Wang et al., "Strain-induced phonon shifts in tungsten disulfide nanoplatelets and nanotubes," *2D Mater.* **4**, 015007 (2016).
- 26) N. Perea-López et al., "Photosensor device based on few-layered WS₂ films," *Adv. Funct. Mater.* **23**, 5511 (2013).
- 27) B. Groven et al., "Chemical vapor deposition of monolayer-thin WS₂ crystals from the WF₆ and H₂S precursors at low deposition temperature," *J. Chem. Phys.* **150**, 4703 (2019).
- 28) B. Groven et al., "Two-dimensional WS₂ crystals at predetermined locations by anisotropic growth during atomic layer deposition," *J. Appl. Phys.* **128**, 5302 (2020).